CMES, vol.75, no.4, pp.247-264, 2011

# A Hybrid Quantum-Classical Simulation Study on Stress-Dependence of Li Diffusivity in Graphite

**N. Ohba[1,2], S. Ogata[2], T. Tamura[2], S. Yamakawa[1] and R. Asahi[1]**

**Abstract:** Understanding the stress dependence of Li diffusivity in the Li-graphite intercalation compound (Li-GIC) that has been used in the Li-ion rechargeable battery as a negative electrode, is important to search for better conditions to improve the power performance of the battery. In the Li-GIC, the Li ion creates a long-ranged stress field around itself by expanding the inter-layer distance of the graphite. To take into account such a long-ranged stress field in the first-principles simulation of the Li diffusion, we develop the hybrid quantum (QM)-classical (CL) simulation code. In the hybrid code, the QM region selected adaptively around the Li ion following its motion is treated with the real-space density-functional theory. The rest of the total system is described with an empirical inter-atomic potential that includes a novel formula for the dispersion force between the C atoms that belong to different layers. A series of the hybrid QM-CL simulation runs for the dynamics of a single Li-ion in the graphite are performed at temperature 423 K for various values of the averaged inter-layer distance. We thereby find that the Li diffusivity is suppressed substantially when the inter-layer distance is compressed by a few percent from the equilibrium value. On the other hand, the Li diffusivity is unaffected by the stretching of the inter-layer distance up to a few percent. In the equilibrium and stretched cases, the diffusive motion of the Li ion is composed of ballistic and hopping modes. In the compressed case, the Li ion diffuses in the hopping mode only and is confined in a small area at long times. Separately the activation energy for the hopping diffusion is calculated at zero temperature to find that it is as small as 0.1 eV and that the substantial contribution comes from the deformation energy of the whole system. Based on the findings we propose a mechanism to explain the unique Li-density dependence of the Li diffusivity observed experimentally in the Li-GIC.

**Keywords:** Li-graphite intercalation compound, Li ion, hybrid simulation, density-

---

[1] Toyota Central Research & Development Laboratories, Inc., Nagakute, Aichi 480-1192, Japan

[2] Graduate School of Engineering, Nagoya Institute of Technology, Gokiso-Cho, Showa-ku, Nagoya 466-8555, Japan

functional theory, diffusivity, stress dependence, Li-ion battery

## 1 Introduction

The graphite can form various intercalation compounds by incorporating atoms (ions) and small molecules between its layers. The lithium (Li)-graphite intercalation compound (Li-GIC) is put to practical use as a negative electrode of the Li-ion rechargeable battery. In the battery, the Li ions are shuttled between the positive and negative electrodes by the applied voltage through the non-aqueous electrolyte and separator. Such charge-discharge reactions in the Li-ion battery involve following key processes: the transport of the Li ions in both electrode and electrolyte materials, the charge transfer at the electrolyte-electrode interfaces, and the internal structural changes of the electrodes as the Li density is increased. Much interest exists to advance the power, capacity, and durability of the Li-ion battery relating to the recent electric power saving and environmental problems. Among the key processes, the transport process of the Li ions in the graphite layers is related directly to the power performance of the Li-ion batteries. We will address the problem of the Li diffusivity in the graphite at finite temperatures by exploiting the concurrent-type hybrid simulation technique developed recently. Our investigation of the Li diffusivity in the graphite is not only interesting as a fundamental physical process but also important to design advanced Li-ion batteries.

It is well known that the inter-layer distance of the Li-GIC expands by about 10% with the insertion of the Li: for instance, the distance is 3.35 Å for pure graphite, while 3.70 Å for $LiC_6$ [Kganyago and Ngoepe (2003)]. We here note that the Li-GIC transforms among various microscopic structures [Ohzuku, Iwakoshi, and Sawai (1993)] accompanied with the change in the layer-stacking sequence as the averaged Li-density increases: the random-stage structure is seen at low Li-density, the stage-4 structure that denotes the existence of four C-layers between the inserted Li-layers at a higher Li-density, the stage-3 structure at a much higher Li-density, etc.; the AB sequence at low Li-density, while the AA sequence at high Li-density as in $LiC_6$. Owing to the high stiffness of the C-layer in parallel to the layer surface, those structural and sequential changes of the Li-GIC should extend to the long range. The expansion around the Li ion mentioned above creates the stress field in the C layers, which should affect the Li diffusivity. The relation between the Li diffusivity and the stress field is expected also for the following situation. Since the layers of the graphite are easy to be compressed or stretched due to their weak C-C interaction through the dispersion force, it is natural to expect that the Li ion may diffuse slower or faster when the graphite is pushed or pulled, respectively. Despite the fundamental importance of the issue, no quantitative evidences have been reported about the possible stress (or inter-layer distance) dependence of the

Li diffusivity either from experiments or simulations.

Motivated by those, in the present paper, we will investigate the relation between the Li diffusivity and inter-layer distance of the graphite by the hybrid quantum (QM)-classical (CL) simulation method [Ogata, Lidorikis, Shimojo, Nakano, Vashishta, and Kalia (2001); Ogata, Shimojo, Kalia, Nakano, and Vashishta (2002); Ogata, Abe, Ohba, and Kobayashi (2010)]. The hybrid QM-CL simulation method has been attracting great attention as it is one of the methods that aim to treat large-scale atomistic system with high physical accuracies. In the hybrid method, the QM region whose electronic structures are calculated explicitly by the first-principles method as the density-functional theory (DFT) is embedded in a CL system of atoms that uses an empirical inter-atomic potential model. In the present study, we consider a single Li-ion inserted in the graphite; the total system is charge neutral. The QM region that includes the inserted Li and neighboring C atoms is treated by the DFT implemented in real space. The CL method that uses an empirical inter-atomic potential is applied to the rest of the graphite. The buffered cluster method [Ogata (2005)] is adopted to couple the QM and CL regions dynamically.

Remarkable merits of using the hybrid QM-CL method for the present simulation of the Li ion in the graphite are the following. (i) The hybrid QM-CL method can investigate the diffusion process of the Li-GIC with the influence of surrounding C atoms taken into consideration at a reasonable computational cost. On the other hand, the CL molecular dynamics (MD) method cannot describe generally the chemical reactions such as the charge transfer between the Li and C atoms. Also the first-principles MD method that uses the DFT for electronic structure calculation cannot treat a large-scale graphite system required to study the migration of the Li ion. (ii) The dispersion forces for the inter-layer interaction of the graphite can be incorporated easily through the CL inter-atomic potential model in the hybrid QM-CL method. Remember that the dispersion force cannot be taken into consideration in the conventional DFT method. (iii) It is not necessary to construct an empirical inter-atomic potential between the Li and C atoms. If we succeed to construct the proper inter-atomic potential between the Li and C, we can simulate the Li diffusion in the Li-GIC by the CL-MD method. However, as we will show in §3, the activation energy for the Li diffusion is quite small. It is not easy to construct a precise potential between the Li and C atoms for our purposes.

The rest of the present paper is organized as follows. In §2, we will describe briefly the simulation method and system. Section 3 will report the simulation results on the Li dynamics in the graphite at various settings. We will discuss about the relation between the inter-layer distance and the Li diffusivity. Possible explanation for the significant lowering of the Li diffusivity observed experimentally at the situation of mixed stage-structures will be given. We will conclude the present study in §4.

## 2 Hybrid QM-CL simulation method

We apply the hybrid QM-CL simulation method to investigate the thermal diffusion of a single Li-ion in the graphite with both compression and stretching of the averaged inter-layer distance of the graphite. The details of the hybrid QM-CL simulation method can be found in Refs. [Ogata (2005); Kouno and Ogata (2008); Ogata, Abe, Ohba, and Kobayashi (2010)].

### *2.1 Buffered cluster method*

In the hybrid QM-CL simulation method, a cluster of atoms is selected from the total system as the QM region. The Li ion and its surrounding C atoms make the QM region in the present simulation. Artificial dangling bonds therefore form at the QM-CL boundary. Possible influence of the dangling bonds on the electronic states and the atomic forces should be minimized. The link-atom method that uses the hydrogen atoms for termination of the dangling bonds is often adopted to couple the QM and CL regions. Depending on the selection of the QM region, however, using the link atom method results in significant relaxation of the artificial surface of the QM region and unwanted deformation of the whole system from the original configuration. We therefore adopt the buffered cluster method (BCM) [Ogata (2005)], which requires no link-atom and is insensitive to the selection of the QM region. To use the BCM, we put additional atoms of either H or C (i.e., constituent species), called the buffer atoms, at the QM-CL boundaries to terminate the dangling bonds. The positions of the buffer atoms are determined so as to minimize the potential energy of the corresponding cluster in classical calculation under the constraint of fixed classical buffer atoms. Note that the positions of the buffer atoms are not relaxed in the QM calculation. Thereby artificial surface relaxation of the QM region is suppressed in the BCM.

### *2.2 Quantum mechanical calculation*

For the QM calculation in the hybrid QM-CL simulation, we use the real-space DFT method in which the Laplacian operations in the Kohn-Sham and Poisson equations are evaluated with the finite difference method. The real-space DFT is well-suited to the present setting of the free boundary condition in the QM calculation (i.e., the atomic cluster in vacuum). The details of the algorithm were described in Refs. [Ogata, Lidorikis, Shimojo, Nakano, Vashishta, and Kalia (2001); Ogata, Shimojo, Kalia, Nakano, and Vashishta (2002); Shimojo, Campbell, Kalia, Nakano, Vashishta, Ogata, and Tsuruta (2000)]. The Troullier-Martin-type normconserving pseudopotentials [Troullier and Martins (1991)] are used to describe the interaction of the valence electrons and nuclei (ions). The generalized gradient approximation formula introduced by Perdew, Burke, and Ernzerhof [Perdew, Burke, and Ernzerhof (1996)] is adopted to the exchange-correlation energy term. The Kohn-Sham orbitals and Hartree field are represented on the uniform Cartesian mesh points. The fourth-order finite-difference method is used for the Laplacian operation [Chelikowsky, Troullier, and Saad (1994)]. For parallel computation, those data on the mesh points are divided into domains to be stored in the compute nodes. The multi-grid method [Brandt (1977)] is employed for acceleration of the convergence of the long-wavelength components of the data on the mesh points. The grid spacing $h = 0.45$ a.u. (1 a.u. $\approx 0.5292$ Å), which corresponds to the cutoff energy $(\pi/h)^2 \approx 49$ Ry (1 Ry $= 13.6$ eV) in the plane waves DFT method. In addition, the smaller grid spacing of $h/3$ is used only around the atoms.

### *2.3 Classical molecular dynamics calculation*

In the hybrid QM-CL simulation method, the CL-MD calculation is performed for the CL region, that is, the whole system minus the QM region. The velocity Verlet algorithm is used to integrate the Newton's equations of motion for all the atoms (or ions in the QM region). The Brenner's inter-atomic potential [Brenner (1990, 1992)] is adopted for the C atoms of the graphite. We employ the parameter values listed in Table I in Ref. [Brenner (1990)] except for the equilibrium distance. The equilibrium distance is set to 1.33116 Å so that the calculated equilibrium lattice constant of the graphite becomes equal to the one calculated with the QM calculation, which is slightly longer than that in Ref. [Brenner (1990)]. Such a fine tuning of the parameters in the CL potential is necessary in order not to create artificial stress at the QM-CL boundary in the hybrid QM-CL simulation method [Kouno and Ogata (2008)]. In the Brenner-type potential, the cut-off distance of the interaction is 2.0 Å. It means that only the interaction between the nearest neighbor atoms belonging to the same layer is considered. To take into account the interlayer interaction, we construct the following inter-atomic potential model for the dispersion (or the van der Waals) forces between the C atoms to add it to the CL potential:

$$V_{\mathrm{vdW}}(r) = 4\varepsilon \left\{ \left(\frac{\sigma}{r}\right)^{12} - g(Z)\left(\frac{\sigma}{r}\right)^{6} \right\} f(r) \tag{1}$$

with the distance $r$ between the C atoms belonging to different layers. The basic form of $V_{\mathrm{vdW}}(r)$ is that of the Lennard-Jones potential. The $f(r)$ works to cut-off the potential gradually at a long distance. The $g(Z)$ changes relating to the degree of similarity to the AA sequence of the graphite with the coordination number $Z$ of atoms in a neighboring layer for a given atom. The parameters

$\varepsilon = 2.84$ meV and $\sigma = 3.35$ Å are set in order to reproduce the experimental interlayer energy and distance of the graphite, respectively. With the CL inter-atomic potential thereby constructed for C atoms, the elastic constant for the direction perpendicular to graphite layers becomes $c_{33} = 34.5$ GPa, which is in good agreement with the experimental value 36.5 GPa [Blakslee, Proctor, Seldin, Spence, and Weng (1970)].

The hybrid QM-CL simulation will be performed in the micro-canonical ensemble, that is, the total number of atoms, the shape and volume of the simulation box, and the total energy are constant. The velocity scaling, however, will be applied to control the system temperature.

### 2.4 Simulation system

The simulation system is composed of 3072 C atoms and a single Li-ion under the periodic boundary condition as shown in Fig. 1. As will be explained in §3, the charge transfer occurs between the Li and neighboring C atoms, resulting in formation of the $\mathrm{Li}^+$ state. In total, eight C-layers exist. The graphite assumes the AB sequence since we are interested in the situation of low Li-density. A cluster of atoms composed of the Li and the surrounding C atoms belonging to the two sandwiching layers is set to the QM region. The dynamic selection of the C atoms around the Li ion in motion follows the rule to realize sufficient physical accuracies of the atomic forces, which is pre-determined in a way similar to Ref. [Ogata, Abe, Ohba, and Kobayashi (2010)].

To set proper sizes $(L_x, L_y, L_z)$ of the simulation system at a finite temperature $T$, we begin with considering the sizes at $T = 0$ K. Here the $x$- and $y$-axes are set along the layer, while the $z$-axis perpendicular to the layer. The hybrid QM-CL simulation at $T = 0$ K gives $(L_x, L_y, L_z) =$ (34.44 Å, 29.83 Å, 26.97 Å) as the equilibrium values. The $L_x$ and $L_y$ values are the same as those for the pure graphite; the $L_z$ is only 0.1 Å longer than that for the pure graphite. Since the thermal expansion along the layer is quite small, we use the same values of $(L_x, L_y)$ at finite temperatures also. On the other hand, the thermal expansion along the $z$-axis is substantial. As shown in Fig. 2, we find through separate CL-MD simulation that the coefficient of linear thermal expansion of the pure graphite in $z$-direction is $6.7 \times 10^{-5}$ $\mathrm{K}^{-1}$ with the present CL potential. It is in accord with the experimental data of $7.34 \times 10^{-5}$ $\mathrm{K}^{-1}$ [Baskin and Meyer (1955)] and is the same order with another experimental data of $2.7 \times 10^{-5}$ $\mathrm{K}^{-1}$ [Nelson and Riley (1945)]. We assume that the same expansion coefficient can be applied to the present system since the Li density is too small to affect the system size. Therefore, multiplying the linear expansion factor for 423 K to $L_z = 26.97$ Å for $T = 0$, we find the equilibrium value of $L_z = 27.74$ Å for $T = 423$ K.

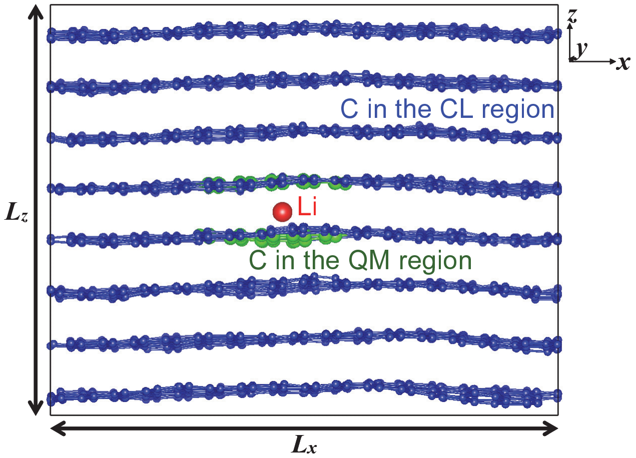

Figure 1: The side ($x-y$) view of the total simulation system. The large red and medium green spheres are respectively the Li and C atoms in the QM region. The small blue spheres are the C atoms in the CL region.

We are interested in the possible effects of change of $L_z$ on the Li diffusivity at $T =$ 423 K. For the compressed situation, we consider $-3.9\%$ and $-1.7\%$ changes in $L_z$ from the original value of 27.74 Å. For the stretched situation, the 2.9% change in $L_z$. In addition, we consider the case of 0.6% change in $L_z$. If we take into account the elongation of 0.35 Å in the inter-layer distance by the Li insertion [Kganyago and Ngoepe (2003)], the resulting $L_z = 27.74 + 0.35 = 28.09$ Å may be taken as the equilibrium value at 423 K. Since $L_z = 27.92$ Å in the 0.6% case is about the middle of the two estimates (27.74 Å and 28.09 Å) for the equilibrium value of $L_z$ at 423 K, we regard the 0.6% case as the equilibrium condition, which relates to the situation of no pressure on the layers.

## 3 Results and discussion

We depict in Fig. 3 the valence-electron density on a $y$-plane in the QM region calculated using the hybrid QM-CL simulation method. The black sphere at around the center of the QM region is the Li ion. The bonding nature between the neighboring C atoms is observed. We find almost no electrons in the vicinity of the Li, indicating significant electron transfer from Li atom to the C atoms to form the $\mathrm{Li}^+$ state.

Figure 4 shows the mean square displacements (MSD) of the Li ion as functions of time in the four cases ($-3.9\%$, $-1.7\%$, 0.6%, and 2.9% changes of $L_z$) at $T =$

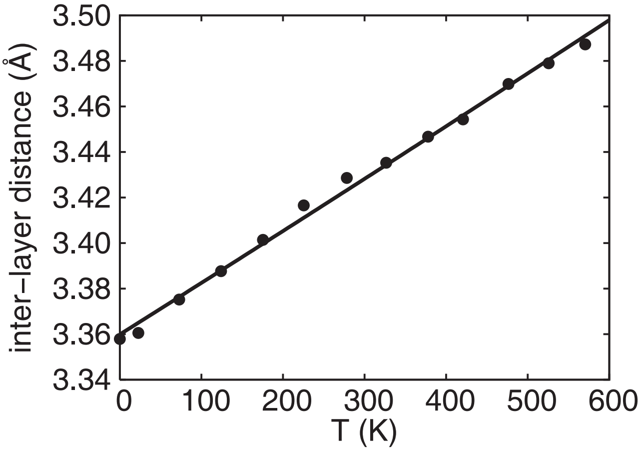

Figure 2: The averaged inter-layer distance of the graphite at equilibrium as a function of temperature $T$ (K), obtained through separate classical MD simulation. The solid line shows the fitting formula $f(T) = 3.36(1+6.7\times 10^{-5}T)$.

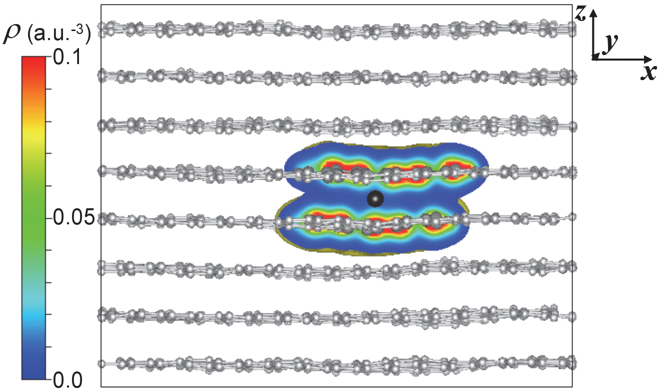

Figure 3: The valence-electron density on a $y$-plane in the QM region obtained in the hybrid QM-CL simulation. The black sphere is the Li ion, while the grey spheres the C atoms. The density less than 0.001 a.u.$^{-3}$ is omitted.

423 K. Since there exists only a single Li-ion in the system, we shift the time origin of the MSD by every 0.1 ps to increase the number of data samples for better statistics. The total simulation time is 12 ps for each run; the time step is 1.0 fs. Therefore the curves in Fig. 4 appear to have substantial fluctuations as the time (i.e., the horizontal axis) gets longer ($t$ >4 ps). The curves in Fig. 4 are not linear enough to estimate the diffusion coefficients at long times. However, characteristic dependence of the Li diffusivity on the change of $L_z$ is observed as follows.

The MSD's for $t = 0 \sim 3$ ps that have small statistical errors, show the clear dependence on $L_z$. As expected, the MSD's in the equilibrium (0.6%) and stretched (2.9%) cases are larger than that in the compressed ($-1.7\%$ and $-3.9\%$) cases. In the equilibrium and stretched cases, we find a super-linear (or partly parabolic) behavior of the MSD as a function of time at short times ($t = 0 \sim 1$ ps), while a linear behavior at longer times ($t = 1 \sim 3$ ps). In the compressed cases, the MSD increases in proportion to time for $t = 0 \sim 3$ ps. The super-linear behavior in the equilibrium and stretched cases indicate a mixture of ballistic and hopping motion of the Li ion. On the other hand, the accurate linear behavior in the compressed cases means the usual hopping motion.

There exist insufficient statistics in the MSD data for $t = 4 \sim 10$ ps, resulting in large fluctuations. In the equilibrium and stretched cases, we find no obvious deviation of the MSD from the linear extrapolation of the data for $t = 1 \sim 3$ ps. In a compressed case ($-1.7\%$), the clear change of the MSD from the linear to saturation behavior is observed. We will explain the mechanism of the saturation behavior later in this section in terms of the cage effect.

The trajectory of the Li ion during 10 ps in each run is plotted in Fig. 5; the initial and final positions of the Li ion are depicted with the open arrow and the large red sphere, respectively. The green spheres are the C atoms in the QM region. When the graphite layers assume the equilibrium distance or stretched one, the Li ion migrates over a wide area. On the other hand, the Li ion appears to be confined in the compressed cases, particularly in the $-1.7\%$ case. In the equilibrium and stretched cases (0.6% and 2.8%) in Fig. 5, we observe both hopping and ballistic modes of the Li ion motion. In the hopping mode, the Li ion moves to avoid the places at which two C atoms belonging to different layers assume the same $x-y$ positions (see, Fig. 6). However, as remarked in Fig.5 with black arrows, we find the Li ion in the ballistic mode can pass through such a place. The ballistic motion makes the MSD super-linear or parabolic in time as already pointed out for the 2.9% and 0.6% cases in Fig. 4. Detailed analyses of the ballistic-motion events show that the inter-layer distances at near places of the Li ion toward the direction of its motion are always larger that 3.85 Å. The value 3.85 Å means stretching the inter-layer distance by 0.36 Å (0.27 Å) as compared to the averaged value in the

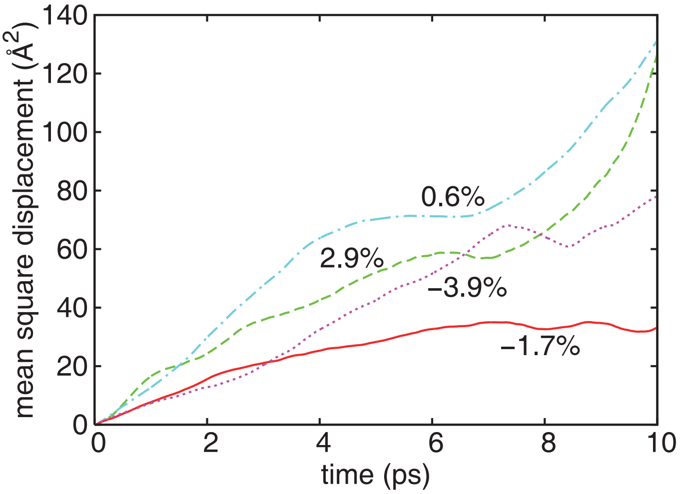

Figure 4: The mean square displacements of the Li ion as functions of time in the hybrid QM-CL simulation at 423 K for the compressed ($-3.9\%$ and $-1.7\%$), equilibrium (0.6%), and stretched (2.9%) values of $L_z$. For better statistics, the time origins are set at every 0.1 ps in the simulation run of total 12 ps.

0.6% (2.9%) case. We, in fact, find that the thermal fluctuation produces such a local stretching frequently at various places in those simulation cases.

In order to understand the mechanisms of the Li diffusivity, the activation energy for the hopping diffusion of the Li ion is evaluated using the hybrid QM-CL simulation method. Figure 6 depicts the positions of the Li ion in the ground state (GS) and the transition state (TS). The activation energy, which is calculated by subtracting the energy in the GS from that in TS, in each case of the $L_z$ change is plotted in Fig. 7. The activation energy obtained from the total energy, i.e., the filled sphere in Fig. 7, includes both contributions of the QM and CL regions. We find that the activation energy is quite small, less than 0.07 eV, irrespective of $L_z$. Therefore, the Li ion can diffuse easily by the thermal fluctuation. As the inter-layer distance becomes shorter, the activation energy estimated from the total energy increases substantially, which supports our finding of suppressed diffusivity by compression.

The contribution of the QM region (i.e., around the Li ion) to the activation energy changes little when the system is compressed or stretched. On the other hand, the contribution of the CL region (far from the Li ion) increases as the system is compressed, which means that the distortion of the C atoms far from the Li ion affects the activation energy. Note that the major contribution to the activation

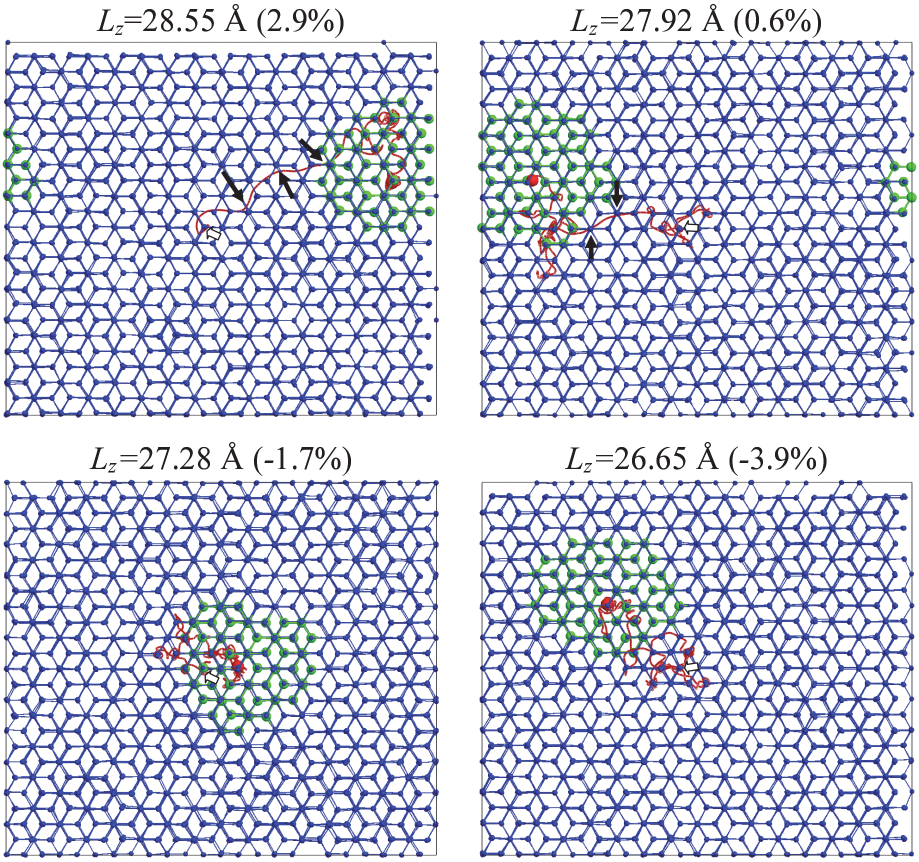
$L_z$=28.55 Å (2.9%)

$L_z$=27.92 Å (0.6%)

$L_z$=27.28 Å (-1.7%)

$L_z$=26.65 Å (-3.9%)

Figure 5: The trajectory of the Li ion during 10 ps viewed from $z$-direction, obtained in the hybrid QM-CL simulation. The four cases of the change of $L_z$ are considered. The initial position of the Li ion is depicted by the open arrow. The final position by the large red sphere. The green spheres are the C atoms in the QM region. The black arrows depict the places where the Li ion passes through the places at which two C atoms belonging to different layers assume the same $x-y$ positions.

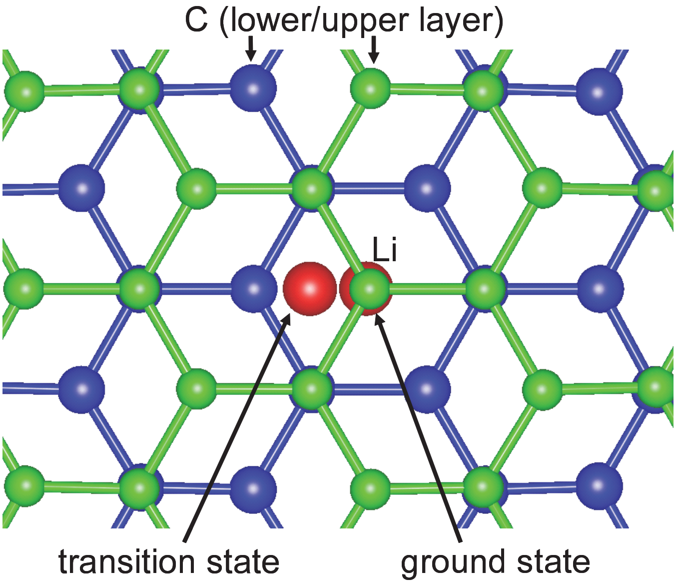

Figure 6: The Li ion at the ground and transition states in the hopping diffusion in the graphite. The Li ion is sandwiched by two C-layers.

energy in compressed system comes from the CL region as seen in Fig. 7. Since the long-ranged distortion is formed in cooperation with a large number of C atoms, the deformation field cannot change in a short time. We guess that such a relatively long-lived deformation field works as a cage for the motion of the Li-ion, resulting in a relatively small migration area as observed clearly in the compressed case ($-1.7\%$) in Fig. 5.

The DFT calculation [Qi, Guo, Louis G. Hector, and Timmons (2010)] reported that the elastic constant $c_{33}$ of the Li-GIC relating to the deformation perpendicular to the layers, increases with increasing the Li density. It is therefore reasonable to consider that the region around the Li ion is hard to be compressed in comparison to the one without the Li. Using the hybrid QM-CL simulation method, we calculate the local strain of the inter-layer distance at both nearby and far regions of the Li ion in the graphite at $T = 0$ K. The standard inter-layer distance at $T = 0$ K is evaluated from the equilibrium distance of the graphite system size $L_z = 26.97$ Å irrespective of regions. The local strain for a given $L_z$, calculated in reference to the standard value, is plotted in Fig. 8. The local strain at the far region changes in proportion to $L_z$. On the other hand, the local strain at the nearby region changes differently. The gradient of the slope with respect to $L_z$ indicates that (i) the nearby region is

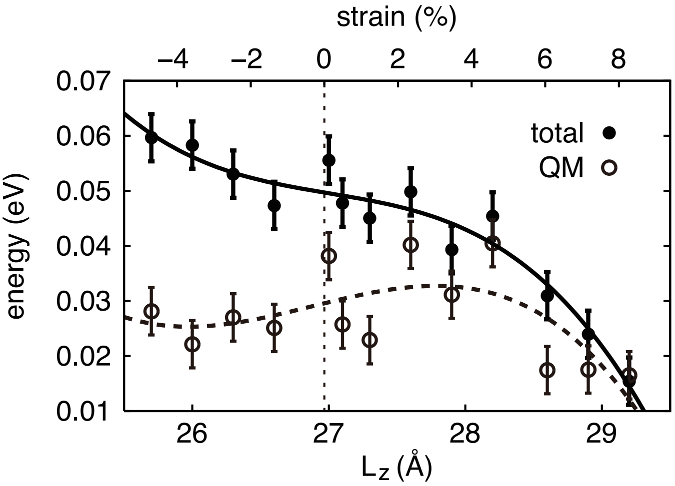

Figure 7: The activation energy for the hopping diffusion of the Li ion in the graphite at $T = 0$ K calculated using the hybrid QM-CL simulation method. The filled circles with the black curve represent the data evaluated using the total energy. The open circles with the gray curve represent the data using the energy of the QM region only. The strain corresponds to the variation of $L_z$ from the equilibrium distance of 26.97 Å at 0 K. The error bars indicate the estimated overall errors relating to the convergence fluctuation in the real-space DFT method.

harder than the pure graphite for $L_z < 26.97$ Å; (ii) it is softer for $L_z = 26.97 \sim 27.6$ Å (iii) it has similar stiffness for $L_z = 27.6 \sim 28.2$ Å. The finding (i) means the accumulation of the deformation energy in the far regions relating to its relative softness when the system is compressed. It is the reason of substantial contribution of the far region to the activation energy in the compressed situation. The similar finding of the substantial contribution of the peripheral (CL) region to the activation energy in the highly strained situation has been reported for the activation energy of the O atom in the Si crystal [Kouno and Ogata (2008)].

To analyze possible error in the activation energy, we calculate the energy with a different method in a similar setting. We use the projector augmented wave method for the DFT calculation implemented in the VASP code [Kresse and Furthmüller (1996)], which is expected to have higher accuracy since the core electrons are treated also in addition to the valence electrons. We prepare the supercell, $3 \times 3 \times 2$ of the unit cell, of the graphite in the AB-sequence. Then a single Li atom is inserted. Hence the total system contains 72 C atoms and 1 Li atom. The supercell and all the atomic positions are relaxed in the GS; and the positions of the C atoms

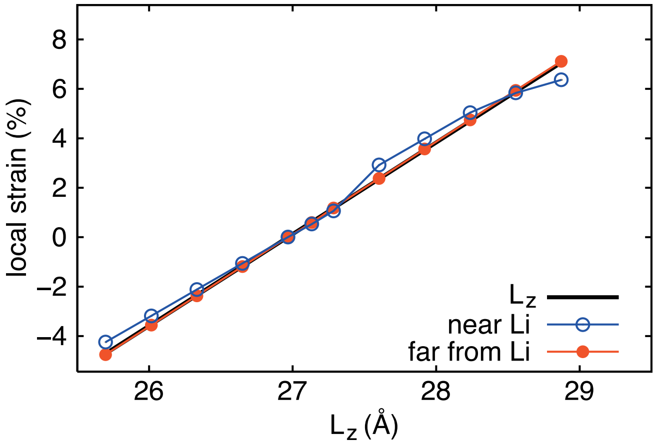

Figure 8: The local strains as functions of $L_z$ calculated using the hybrid QM-CL simulation method at $T = 0$ K. The open blue spheres are for the region near the Li ion; the filled red spheres, for the region far from the Li ion. The black line represents the ideal case of uniform strain.

in the TS. The calculated results by the VASP are listed in Table 1 for both GS and TS. The activation energy evaluated from the electronic energy is 0.09 eV, which is the same order of 0.05 eV obtained by the hybrid QM-CL simulation method at zero strain. Considering the difference in the target system used in the two methods, we state that no substantial difference in the activation energy exists between the two results. In addition we calculate the activation free-energy using the phonon package MedeA [Parlinski (2002)]. Relatively large contribution of the phonon entropy $T\Delta S = -0.14$ eV is found at 400 K. Finally the difference in the Gibbs free-energy between the GS and TS becomes 0.04 eV.

It is known experimentally that the drastic lowering to one severalth of the Li diffusivity occurs in the Li-GIC at particular values of the Li density that correspond to the coexistence of different stage-structures [Funabiki, Inaba, Ogumi, Yuasa, Otsuji, and Tasaka (1998)]: random (dilute)-stage and stage-4, stage-4 and stage-3, etc. From our findings about the stress-dependence of the Li diffusivity in the graphite explained above, we can propose a possible mechanism for the drastic lowering of the Li diffusivity as follows. Suppose a phase boundary in the Li-CIC in which one phase assumes the dilute random-stage and another does the stage-4, as illustrated in Fig. 9. The X-ray diffraction measurement showed that the averaged inter-layer distance gets longer as the stage structure advances relating to the increase in the Li density [Takami, Satoh, Hara, and Ohsaki (1995)]. Therefore,

Table 1: The results of various quantities at the ground state (GS) and transition state (TS) calculated using the VASP code. The $E_{\mathrm{ele}}$, $E_{\mathrm{vib}}^{400\mathrm{K}}$, $S_{\mathrm{vib}}^{400\mathrm{K}}$, and $G^{400\mathrm{K}} = E_{\mathrm{ele}} + E_{\mathrm{vib}}^{400\mathrm{K}} + pV - TS_{\mathrm{vib}}^{400\mathrm{K}}$ are the electronic energy at $T = 0$ K, the vibrational energy including the zero-point energy, the phonon entropy, and the Gibbs free-energy at $T = 400$ K, respectively. The electronic energy is measured in reference to the standard states of the atomic elements.

| | $E_{\mathrm{mele}}$ (eV) | $pV$ (eV) | $E_{\mathrm{vib}}^{400\mathrm{K}}$ (eV) | $S_{\mathrm{vib}}^{400\mathrm{K}}$ (eV/K) | $G^{400\mathrm{K}}$ (eV) |
|---|---|---|---|---|---|
| GS | −7.94 | 2.79 | 13.88 | 0.0063 | 6.22 |
| TS | −7.85 | 2.74 | 13.75 | 0.0059 | 6.26 |
| Δ (TS-GS) | 0.09 | −0.06 | −0.13 | −0.00036 | 0.04 |

due to the relative elongation of the averaged inter-layer distance in the stage-4 phase, compressive and stretching stresses work on average on the stage-4 and the random-stage sides, respectively, at the phase boundary (see, Fig. 9). We have demonstrated in Fig. 4 that only 2% compression in $z$-direction suppress the Li diffusivity substantially: the MSD in the $-1.7\%$ case is about one third of that in the 0.6% case. The compressive stress in the stage-4 side of the phase boundary may play a role to create a confining bank for the Li diffusion. If such a phase boundary extends to the entire system, significant lowering of the Li diffusivity should result.

Remarks on the proposed mechanism for the drastic lowering of the Li diffusivity at the stage-mixture situation are in order. (i) Though difference exists about the layer-stacking between the AA sequence around the Li-rich layers in the stage-4 structure and the AB sequence assumed in our simulation runs, we expect a similar suppression of the Li diffusivity due to compression occurs also in the stage-4 structure. (ii) Since the Li insertion expands the inter-layer distance by about 10%, the 2% compression of the averaged inter-layer distance that we just mentioned can be realized. (iii) Compressive stress also emerges in the random-stage side for the neighboring two layers with the Li ions inserted on the random-stage side and no Li ion on the stage-4 side, as illustrated in Fig. 9. However, because of the relatively low density of the Li ions in the random-stage structure as compared to the stage-4 structure, the Li ions in the random-stage structure should be affected little by such a compressive stress. Rather, the exclusive volume effect [Safran and Hamann (1979)] that causes repulsive interaction between the Li ions located just above and below a graphite layer should lower the Li diffusivity. In fact, the Li diffusivity decreases as the Li density increases in the random-stage [Funabiki, Inaba, Ogumi, Yuasa, Otsuji, and Tasaka (1998)]. (iv) In reality the graphite layers often warp and bend, which means the existence of mixture of the AA- and AB-

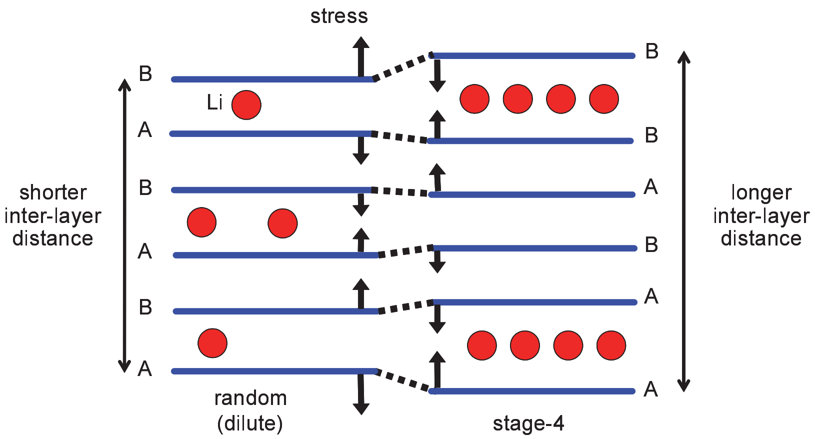

Figure 9: Schematic illustration of the phase boundary of the random-stage and stage-4 structures in the Li-GIC. The blue horizontal lines indicate the graphite layers. The stresses acting on the layers due the differences in the inter-layer distance, are depicted by the arrows.

sequences. Since the inter-layer distance is larger by 4% in the AA-sequence than in the AB-sequence, similar mechanism for the Li diffusivity may work also for this situation.

In all the simulation runs explained in the present paper, only a single Li-ion in the graphite is treated, in other words, mutual interaction between the Li ions is ignored. As already pointed out in Ref. [Safran and Hamann (1979)] as the exclusive volume effect, the Li-Li interaction should affect the Li diffusivity. We are working on the issue by performing a larger scale hybrid QM-CL simulation, in which neighboring Li ions and their surrounding C atom are treated together as a single QM region. Such a large QM region is treated by our novel divide-and-conquer-type order-$N$ DFT method to be reported in a separate paper. Combined effects of the external stress and the Li-Li interaction will be clarified.

## 4 Conclusion

We have applied the hybrid QM-CL simulation code to analyze the stress dependence of the diffusivity of a single Li-ion in the graphite at $T = 423$ K by changing the averaged inter-layer distance (by plus and minus a few percent). The real-space DFT method has been applied to treat the QM region that is selected adaptively to include the Li and its surrounding C atoms. The weak C-C interaction (i.e., the dispersion force) acting between different C-layers has been modeled through the CL inter-atomic potential. Thereby we have found that the Li diffusivity is suppressed significantly in the compressed case, while no substantial change is observed in the stretched case. In the stretched case, the Li-ion motion has shown both hopping and ballistic modes. On the other hand, in the compressed case, the Li ion has diffused through the hopping mode only and has been found to be confined in a relatively small area at longer times; its mechanism has been explained in terms of the cage effect. The activation energy for the hopping diffusion has been found as small as 0.1 eV at $T = 0$ K, in accordance with the fast thermal diffusion of the Li ion observed in the present simulation. From our findings about the stress-dependence of the Li diffusivity in the graphite, we have proposed a possible mechanism for the drastic lowering of the Li diffusivity at particular densities of Li observed experimentally in the Li-CIC.

**Acknowledgement:** We thank Dr. R. Kobayashi and Dr. S. Hyodo for helpful discussions. The present work was supported in part by JST-CREST, JSPS-KAKENHI (233100074).

## References

**Baskin, Y.; Meyer, L.** (1955): Lattice constants of graphite at low temperatures. *Physical Review*, vol. 100, no. 2, pp. 544.

**Blakslee, O. L.; Proctor, D. G.; Seldin, E. J.; Spence, G. B.; Weng, T.** (1970): Elastic constants of compression-annealed pyrolytic graphite. *Journal of Applied Physics*, vol. 41, no. 8, pp. 3373–3382.

**Brandt, A.** (1977): Multi-level adaptive solutions. *Mathematics of computation*, vol. 31, no. 138, pp. 333–390.

**Brenner, D.** (1990): Empirical potential for hydrocarbons for use in simulating the chemical vapor deposition of diamond films. *Physical Review B*, vol. 42, no. 15, pp. 9458.

**Brenner, D.** (1992): Erratum: Empirical potential for hydrocarbons for use in simulating the chemical vapor deposition of diamond films [phys. rev. b 42, 9458 (1990)]. *Physical Review B*, vol. 46, pp. 1948.

**Chelikowsky, J. R.; Troullier, N.; Saad, Y.** (1994): Finite-difference-pseudopotential method: Electronic structure calculations without a basis. *Phys. Rev. Lett.*, vol. 72, no. 8, pp. 1240–1243.

**Funabiki, A.; Inaba, M.; Ogumi, Z.; Yuasa, S.; Otsuji, J.; Tasaka, A.** (1998): Impedance study on the electrochemical lithium intercalation into natural graphite powder. *Journal of The Electrochemical Society*, vol. 145, no. 1, pp. 172–178.

**Kganyago, K.; Ngoepe, P.** (2003): Structural and electronic properties of lithium intercalated graphite lic$_6$. *Physical Review B*, vol. 68, no. 20, pp. 205111.

**Kouno, T.; Ogata, S.** (2008): Activation energy for oxygen diffusion in strained silicon: A hybrid quantum-classical simulation study with the nudged elastic band method. *Journal of the Physical Society of Japan*, vol. 77, no. 5, pp. 054708.

**Kresse, G.; Furthmüller, J.** (1996): Efficient iterative schemes for ab initio total-energy calculations using a plane-wave basis set. *Phys. Rev. B*, vol. 54, no. 16, pp. 11169–11186.

**Nelson, J.; Riley, D.** (1945): The thermal expansion of graphite from 15° c. to 800°c.: part i. experimental. *Proceedings of the Physical Society*, vol. 57, pp. 477.

**Ogata, S.** (2005): Buffered-cluster method for hybridization of density-functional theory and classical molecular dynamics: Application to stress-dependent reaction of h$_2$ o on nanostructured si. *Physical Review B*, vol. 72, no. 4, pp. 045348.

**Ogata, S.; Abe, Y.; Ohba, N.; Kobayashi, R.** (2010): Stress-induced nano-oxidation of silicon by diamond-tip in moisture environment: A hybrid quantum-classical simulation study. *Journal of Applied Physics*, vol. 108, pp. 064313.

**Ogata, S.; Lidorikis, E.; Shimojo, F.; Nakano, A.; Vashishta, P.; Kalia, R.** (2001): Hybrid finite-element/molecular-dynamics/electronic-density-functional approach to materials simulations on parallel computers. *Computer Physics Communications*, vol. 138, no. 2, pp. 143–154.

**Ogata, S.; Shimojo, F.; Kalia, R.; Nakano, A.; Vashishta, P.** (2002): Hybrid quantum mechanical/molecular dynamics simulation on parallel computers: density functional theory on real-space multigrids. *Computer physics communications*, vol. 149, no. 1, pp. 30–38.

**Ohzuku, T.; Iwakoshi, Y.; Sawai, K.** (1993): Formation of lithium-graphite intercalation compounds in nonaqueous electrolytes and their application as a negative electrode for a lithium ion (shuttlecock) cell. *Journal of the Electrochemical Society*, vol. 140, pp. 2490.

**Parlinski, K.** (2002): Medea-phonon, materials design, inc., 2003, based on k. parlinski, phonon 3.11, 2002.

**Perdew, J. P.; Burke, K.; Ernzerhof, M.** (1996): Generalized gradient approximation made simple. *Phys. Rev. Lett.*, vol. 77, no. 18, pp. 3865–3868.

**Qi, Y.; Guo, H.; Louis G. Hector, J.; Timmons, A.** (2010): Threefold increase in the young's modulus of graphite negative electrode during lithium intercalation. *Journal of The Electrochemical Society*, vol. 157, no. 5, pp. A558–A566.

**Safran, S. A.; Hamann, D. R.** (1979): Long-range elastic interactions and staging in graphite intercalation compounds. *Phys. Rev. Lett.*, vol. 42, no. 21, pp. 1410–1413.

**Shimojo, F.; Campbell, T. J.; Kalia, R. K.; Nakano, A.; Vashishta, P.; Ogata, S.; Tsuruta, K.** (2000): A scalable molecular-dynamics algorithm suite for materials simulations: design-space diagram on 1024 cray t3e processors. *Future Generation Computer Systems*, vol. 17, no. 3, pp. 279 – 291.

**Takami, N.; Satoh, A.; Hara, M.; Ohsaki, T.** (1995): Structural and kinetic characterization of lithium intercalation into carbon anodes for secondary lithium batteries. *Journal of The Electrochemical Society*, vol. 142, no. 2, pp. 371–379.

**Troullier, N.; Martins, J. L.** (1991): Efficient pseudopotentials for plane-wave calculations. *Phys. Rev. B*, vol. 43, no. 3, pp. 1993–2006.